## Title

Air-permeable textile bioelectronics for wearable energy harvesting and active sensing



## Author

Chang, Austin

## Publication Date

2022

Peer reviewed|Thesis/dissertation

UNIVERSITY OF CALIFORNIA

Los Angeles

# Air-permeable textile bioelectronics for wearable energy harvesting and active sensing

A thesis submitted in partial satisfaction

of the requirements for the degree Master of Science

in Bioengineering

by

Austin Chang

2022

ABSTRACT OF THE THESIS

Air-permeable textile bioelectronics for wearable energy harvesting and active sensing

by

Austin Chang

Master of Science in Bioengineering

University of California, Los Angeles, 2022

Professor Jun Chen, Chair

Advances in wearable bioelectronics enable changes in the current reactive and disease-centric healthcare system to a personalized model, focused on disease prevention and health promotion. Harnessing the body's biomechanical forces is a unique way to develop wearable bioelectronics for personalized healthcare. The research advancements in triboelectric nanogenerators and their ability to produce electrical signals in the presence of deformation, compression, and bending, among other movements have made it very favorable for miniaturized biomechanical motion sensors. In this work, we developed a soft triboelectric nanogenerator (S-TENG) formed with a liquid metal electrode treated with Nickel (Ni-EGaIn) encapsulated between two layers of Polycaprolactone (PCL) electrospun textiles. The Ni-EGaIn liquid demonstrates more tunable characteristics with a viscosity of 2,786 Pa·s at a shear rate of 1 $s^{-1}$. The PCL cloth effectively wicks moisture keeping the sensor dry and cool with a drying rate of 5.07 % $min^{-1}$ compared to conventional fabrics such as polyester with

a drying rate of 3.93 % $min^{-1}$. Operating as a single-electrode, the 4x4 $cm^2$ patch demonstrated its ability to produce an open-circuit voltage of 12 V with a short-circuit current of 0.12 mA, ultimately outputting a power density of 7.975 W $m^{-2}$. The S-TENG exhibited stable performance over many cycles and demonstrated its capability in producing electrical output under varying degrees of deformation in the form of stretching and bending. It has the potential to be integrated into all aspects of wearables such as patches, bracelets, and even clothing. The capabilities of the S-TENG given its power output efficiency, economical practicality, as well as user-friendly structure establishes itself as a promising approach to sustainable, wearable bioelectronic devices.

The thesis of Austin Chang is approved.

Tzung Hsiai

Liang Gao

Jun Chen, Committee Chair

University of California, Los Angeles

2022

# TABLE OF CONTENTS

# LIST OF FIGURES

## ACKNOWLEDGEMENTS

I would like to express my gratitude to Dr. Jun Chen, for his great mentorship. His enthusiasm for this subject and extensive knowledge and familiarity with this field has played a great role in my interest in wearable bioelectronics. Through meetings, lectures, and coursework, I have learned to think more critically about this subject and gained a greater appreciation for research and academia. Without his positivity and thoughtfulness, I would not have had the motivation to pursue this thesis and research.

Next, I would like to thank Xun Zhao for his mentorship and patience throughout my time in the lab. Given the difficulties and obstacles that came with COVID-19, Xun made sure that I was always making progress and periodically checked in with me. Witnessing his devotion to research and practicality with the work has helped me to grow as a researcher and recognize the many skills I still lack. Through his thoroughness and sincerity as well as encouragement, I have learned a lot about what it takes to be a part of a research team.

In addition, I would like to thank Professor Joe Distefano III and Professor Nathan Tung for giving me the opportunity to TA for their courses. Struggling with financial difficulties, their flexibility to incorporate me into their programs has made this master's program achievable. Their understanding and consideration of my workload have been incredible and something I will not take for granted.

I would also like to thank Dr. Jacob Rosen and Dr. Dino Di Carlo. In my undergrad, I got to do research in these labs. While I spent no more than a year in either, I still learned a lot about how I am as a researcher and more importantly, what kind of research appeals to me. My time working in these two separate labs was certainly not wasted and an incredibly worthwhile experience.

Last, but not least, I would like to thank my friends for their amazing encouragement and support. They have been there for me during the rough moments and celebrated with me during the

good. My friends, especially my roommates, have been understanding of the hours and stress I have experienced both academically in school and mentally in my personal life. I would also like to thank my family for supporting me through my journey at UCLA. Special shoutout to my brother and sister for looking out for me all these years. And to my grandpa – who was one month from finding out I where I was going for college – I would like to thank him for always putting a smile on my face with his never-ending reminders that high education is important.

An additional thanks to everyone in the Chen Wearable Bioelectronics Lab for being welcoming and supportive during my study. I also thank Dr. Tzung Hsiai and Dr. Liang Gao for being my committee members.

# 1. Introduction

Wearable bioelectronics have increased in popularity over the last decade with the rapid advancement of Internet of Things. This improvement in wearable bioelectronics raises the practicality of achieving personalized healthcare. While personalized healthcare is difficult to accomplish for a large population, it has a lot of attractive individual benefits elevating the patient's health[1]. Rather than intermittent monitoring and diagnosing patients during hospital visits, wearable bioelectronics opens the path to continuous monitoring[2], which can assist with the prevention of illness through early diagnostics and detection of problems. It can also provide a wealth of data for analysis across all sorts of conditions related to the patient. With the advances in wearable bioelectronics raising our ability to continuously monitor the body's conditions, there is promising potential for innovation in both tracking and communication, enhancing personalized healthcare.

The increase in demand for wearable bioelectronics capable of monitoring physical performance, in-home care, patient health assessments, and all sorts of applications in connected health has motivated the development of various sensing and power generation approaches[3]. Flexibility to mechanical deformation from biomechanical motion, noninvasiveness, light-weight systems, and portability are all qualities that are highly desired in wearable bioelectronics[4]. Over the last two decades, meeting these criteria has evolved wearable bioelectronics into a newer platform of bioelectronics in the form of wearable textiles[5]. Having been so fully integrated into the daily life of humans for thousands of years, wearable textiles are a very attractive area to explore given their potential to not only perform sensing but also avoid interfering with the activity of the individual due to their comfort and flexibility as well as intrinsically breathability [6-10]. Sensing is very achievable in fabric-based textiles as deformation caused by biomechanical motion can result in electric signal generation. Popular approaches involve electromechanical wearable bioelectronics utilizing

piezoresistive, capacitive, triboelectric, piezoelectric, and magnetoelastic sensing mechanisms[11-18]. Piezoresistive sensors, currently the most prevalent mechanoelectrical sensor[13], perform sensing by making use of yarn[19] or thread [20, 21] as well as textile-based sensing[22, 23] in order to achieve monitoring applications in garments and clothing. Recent studies in capacitive sensors have been applied to respiration monitoring[24], a myriad of body motion activity recognition instances[25], and noncontact health care monitoring in the form of textiles in the shape of a rings[26]. Triboelectric nanogenerator devices have been demonstrated to perform real-time respiration monitoring[27], active gesture sensing[28], and even influenced devices capable of eyeball motion capture [29]. Similarly, piezoelectric bioelectronics have been applied to joint sensing [30] and extensive examples of sensing through electronic textiles [31].

Beyond sensing limitations attributed to the different respective mechanisms, an important consideration for sensors is the power source. Batteries introduce countless issues including a limited lifespan and toxicity to the environment. Also, given their rigid and bulky nature, batteries can introduce weight and discomfort from the sensor to the user [32]. Ideally, sensors need to be flexible, lightweight, and comfortable to properly adapt to the needs of its user. Thus, a replacement for batteries in the form of self-powered energy harvesting devices is desired. Independent, scalable power-generating sources would be the goal as they would be able to sustain the sensors and provide information and data continuously without having to recharge and get in the way. Wearable textiles employing triboelectric nanogenerators [33-39], especially stand out along with piezoelectric nanogenerators [40-44] as both can perform energy harvesting, introducing the opportunity for sustainable, continuous monitoring. Triboelectric nanogenerators are an appealing approach as these sensors make use of simple fabrication methods, cheap material costs, and availability of triboelectric series materials and device designs [45]. Triboelectric generators have gained popularity in the last decade, with research demonstrating their capability of transforming biomechanical motion into an

electrical power [11, 35, 46-49]. Additionally, TENG has the potential to overcome some common sensor challenges such as the ability to perform high-dynamic detection as well as performing static monitoring.

In the process of merging triboelectric nanogenerators (TENG) with our clothing, the selection of the appropriate textile to complement these wearable devices is an important consideration. The soft textile TENG is capable of converting biomechanical motions into electrical signals through the contact and separation of two distinct triboelectric materials [50]. This is an achievable and simple structure that can effortlessly be applied with a wide range of available materials. The flexibility of source textile materials opens the door for more selective criteria focused on comfort and performance. Of the many materials used for fibers including wool, cotton, silk, and linen as well as synthetic textiles from Polyester and nylon, polyethylene (PE) textiles stand out offering a competitive functional performance [9]. Comparable in mechanical properties [51, 52], polyester textile, Polycaprolactone (PCL) is also a promising material. Woven PE and PCL fabrics are economical, have exciting functionality such as cooling capabilities, and have excellent mechanical properties. Both textiles are also biodegradable, biocompatible, and non-toxic making them good candidates for wearable textile consideration.

Similarly, the deliberate selection of an electrode is important for the electric signal and current conduction of the system. It must also be compatible with the wide availability of choices capable of meeting the TENG energy harvesting mechanism requirements. An agreeable approach to match the flexibility desired in the soft textile TENG involves the implementation of an electrode made up of some form of liquid metal. Liquid metal alloys gallium, gallium-indium-tin, and eutectic gallium-indium have gained popularity given their viscoelastic as well as metallic properties at room temperature [53]. They are also a low-toxic alternative to mercury. The liquid metal functions well in its liquid state as it can effectively mold to the design of the sensor [54]. Additionally, the formation

of a stable outer surface oxide layer of "skin" protects the electrode and helps the liquid metal body mechanically stabilize [55].

In this work, we present a flexible, sustainable power source in the form of an air-permeable soft bioelectronics device that is easily reproducible and made out of economically viable materials. The device is lightweight, flexible, and also breathable developed from a fabrication strategy utilizing electrospun technology to form the textile out of polycaprolactone [56]. In terms of sensing and power generation, the device acts as a triboelectric nanogenerator, producing electric signals through the triboelectric effect. The device can easily be implemented into a network of sensing systems in the PCL electrospun cloth achieving biomechanical sensing given its sensitivity to deformation. Combining simple PCL nanofiber mesh cloth with a Ni-doped light liquid metal layer Eutectic Gallium-Indium (EGaIn), a 4 cm by 4 cm air-permeable textile is capable of reliably providing an output power of 7.975 W $m^{-2}$. The lightweight PCL nanofibers when considered with their air-permeability, flexibility, biocompatibility[57], and biodegradability[58] offer a favorable material to house the liquid metal. The PCL itself is appealing as it is nontoxic[59], durable[60], and stable with desirable rheological properties[61, 62]. This device can be adapted to clothing and patches to function not just as an energy harvester, but more importantly, as a biomechanical sensor. Given its discreet and subtle appearance, it can easily be integrated into everyday wear serving its sensing and energy harvesting functions as well as providing comfort and effective moisture wicking away through its breathability and flexibility [63].

# 1. Results and Discussion

### 2.1 Characterization of liquid metal

To optimize the liquid metal's performance in the overall structure of the S-TENG as a wearable sensor, it is important for it to not only be flexible but also for it to adhere well to the cloth and maintain some semblance of shape and form. In order to do so, the surface tension and adhesivity need to be addressed in the liquid metal composition. This augmentation was done by implementing Nickel (NI)-doping on liquid metal which has been demonstrated to increase oxidation of the EGaIn[64]. This increase in oxidation brings about two main benefits. The accelerated oxidation lowers the surface tension of the EGaIn liquid metal. Additionally, Ni-doped EGaIn can induce greater adhesivity compared with that of regular EGaIn[65]. This adhesivity plays a role in increasing the viscosity of the liquid metal. While the liquid flexibility of the metal electrode leads to greater flexibility in the sensor, there needs to be a balance. A degree of viscosity must also be considered as it is necessary to maintain some form and shape in the electrode. Hence, by adding nickel the viscosity increases, providing another valuable characteristic to the electrode. This behavior is shown when testing the mechanical properties of the Ni-EGaIn. We started by mixing the Nickel with the EGaIn liquid metal (Fig. 1a). We compared the Ni-EGaIn with purely just the EGaIn liquid metal itself through a series of mechanical tests by rheometer (Fig. 1b). The apparent viscosity increases in the Ni-EGaIn in comparison with regular EGaIn (Fig. 1c). This indicates that the Ni-EGaIn will be easily processed as an electrode since it is more viscous. As shown in the storage modulus (Fig. 1d) and loss modulus (Fig. 1e) tests, doping liquid metal with Ni particles increases both the storage modulus as well as the loss modulus. It is worth noting that as the shear stress approaches 100 Pa, undoped EGaIn experiences a more drastic drop in its storage modulus falling lower than its loss modulus while the doped EGaIn maintains a steadier storage modulus value and sees significant drops closer to shear

stresses of just under 1000 Pa. These results indicate that beyond simply being able to conduct electricity for the sensor, the sensors also gain structural benefits. In this form, the liquid metal will have an improved material mechanical strength while simultaneously still maintaining an elastic-material-like quality given that the storage modulus is higher than that of the loss modulus.

**2.2 Characterization of the PCL electrospun cloth**

One of the key components of the S-TENG is the fabric material that acts as the primary interface between the user and the liquid metal electrode. The intention of this cloth is to be able to enable triboelectrification when interacting with the electrode while simultaneously retaining desirable wearable fabric qualities such as air permeability, drying capabilities, and flexibility. For this experiment, Polycaprolactone (PCL) was dissolved and underwent the process of electrospinning to prepare the PCL microfibers for use (Fig. 2a). To investigate the mechanical properties of the cloth itself, stress-strain tests were performed (Fig. 2b). In terms of mechanical strength and performance and resistance under stress, the Young's modulus of the fabric was measured to be 1.58 MPa. The fabricated PCL cloth is depicted in the photographic image in Fig. 2c, exhibiting soft, flexible, and lightweight physical qualities. We also investigated the microstructure of the PCL electrospun cloth by fluorescence microscope, which indicates the dispersion of the microfibers (Fig. 2d). In the process of the development of the PCL cloth for the S-TENG , varying mesh sizes of the woven cloth were tested. The morphology of these iterations of the PCL cloth was then examined through scanning electron microscopy (SEM). Imaged mesh cloth sizes with18, 35, and 70 mesh were demonstrated at an unstretched state (Fig. S1). For the 18-mesh cloth, the lateral dimensions were measured to be 630 μm by 710 μm (Fig. S1a). The lateral dimensions for the 35-mesh cloth were 300 μm by 250 μm (Fig. S1b). And finally, the lateral dimensions for the 70-mesh cloth were 140 μm by 140 μm (Fig. S1c). For the assembly of the S-TENG, 120 mesh PCL cloth was selected for its finely-designed micro-structure

with enhanced contact area to increase triboelectrification[66]. The microfibers are evenly dispersed in these magnified views and nicely stacked on top of each other (Fig. 2e, 2f). The measured average diameter of the fibers is approximately 1.6 μm (Fig. 2g). A final adjustment to the cloth was to improve its drying properties. Removing sweat from the skin provides comfort and is typically a two-step process in which the moisture on the skin is wicked by the fabric before evaporating from the cloth. Untouched and unchanged, the PCL cloth without any sort of treatment will not have efficient wicking capabilities (Fig. S2). Due to high surface energy, water in the form of droplets will stick to the cloth and not easily evaporate. To enhance the drying ability of the PCL cloth, the fabric was put through plasma treatment to lower the surface energy. The subsequent behavior resulted in a droplet wicking within 5 seconds (Fig. 2h,2i). This efficient spreading of the droplet through wicking would then increase the area in which the water droplet is exposed accelerating the rate of evaporation. When used in modern applications, this would increase the comfort of the fabric making it more suitable for wear as it can more easily remove sweat from the body through the process of wicking and evaporation.

As previously mentioned, the EGaIn liquid metal was mixed (doped) with nickel particles. For the implementation of the electrode into the S-TENG , polyethylene terephthalate (PET) was used to pattern the liquid metal electrode. A PET mask was placed on a surface over a magnet (Fig. 2j). A laser was then used to burn through the PET mask patterning grooves into the thin film acting similar to a mold (Fig. 2k). Finally, a layer of the PCL cloth was placed underneath the PET mask and the EGaIn liquid metal was poured on top in the patterned spaces of the PET, consequently coming into contact with the PCL cloth and oxidizing (Fig. 2l). The magnet below the surface was used to keep the liquid metal in place given its fluidity. Finally, the PET is removed, and a second PCL cloth is placed over the liquid metal. Altogether, after optimizing the PCL electrospun cloth with plasma treatment and implementing the Ni-EGaIn liquid metal consisting of roughly 10% of the overall

fabric area, the S-TENG textile was constructed (Fig. 2m). The assembly of the S-TENG is made up of printed EGaIn liquid metal electrodes sandwiched between two PCL electrospun cloths. The PCL textile has a high negative electron affinity; thus, it can provide desired characteristics of wearable electronic textiles. Its electron affinity allows for the potential difference between the cloth and the liquid metal to promote the process of triboelectrification. The electrospun cloth structure while holding the electrode between the two cloths, can maintain the desired flexible and adaptable shape while simultaneously retaining its porous, breathable attributes.

**2.3 Characterization of S-TENG as a Power Source**

The S-TENG relies on two main motions to generate electricity (Fig. 3a). Under pressure from skin contact, bending, or tapping will induce vertical contact separation of the triboelectric nanogenerator. Contact between the two triboelectric materials, the electrode, and the PCL cloth will cause coupling of triboelectrification and electrostatic induction. When the skin puts pressure on the S-TENG , the contact between the electrode and PCL will induce more negative charges in the cloth closer to the metal and more positive charges in the zone of the electrode closer to the cloth. The continuous separation and contact of the two materials will then result in a change in potential resulting in which electrons can flow in and out of the electrode which is connected to a wire to ground. This flow of electrons results in a current, thus creating the mechanism for power generation. As illustrated in Fig. 4b, the atoms of the two different materials will start with different charges, but we expect that under the external mechanical forces, as the two atoms draw closer together, the electrons will in turn transfer to a more balanced state.

To understand the capabilities of the S-TENG and its electrical output with different materials, the S-TENG was subjected to contact from various sources including Aluminum, Steel, PET, Kapton, and FEP. (Fig. 3c). Each of these materials has a distinct affinity to either lose or gain electrons through

contact and separation of said materials with the electrospun cloth. The contact and separation induce the triboelectric effect on the PCL giving it varying initial charges which can vary the electrical output of the S-TENG as it then comes in contact with the EGaIn liquid metal electrode. From these tests, the S-TENG demonstrates the capability of having unique signals for different materials in the triboelectric series. In the same way, when human skin meets the S-TENG , it can induce electron transfer as the two surfaces have different electrification, inducing electrification beyond simple mechanical motion between the PCL and the EGaIn electrode. The triboelectrification and electrostatic induction from this simple contact show great potential for application in wearable bioelectronics.

To investigate the conversion from mechanical motion to electrical output, several scenarios were implemented to better understand the S-TENG 's performance. Short-circuit current was measured at increasing frequencies (Fig. 3d). From 1 Hz to 6 Hz tapping frequency, the current increased from 0.008 mA to 0.08 mA. On the other hand, mechanical motion at higher frequencies did not result in any noticeable difference in voltage amplitude and remained within the same range between 2.91 V to 3.62 V even as the tapping frequency sped up from 1 Hz to 6 Hz (Fig. 3e). The electrical output is characterized by increasing current as a result of increasing the frequency of the mechanical motion applied to the fabric over time. This behavior can be explained by the working principle of the bending triboelectric nanogenerator motion. By increasing the rate at which the materials come into contact and then separate, the charges are forced to travel at a faster rate resulting in a greater measured short-circuit current (Fig. 3d). On the other hand, TENG has a restrained inherent material property as well as a range of motion; the charged surfaces due to the triboelectric effect will have an inherent limit to how high they can go. With the same force of tapping, the separation of charges will not increase, thus keeping the open-circuit voltage practically the same, even at higher frequencies (Fig. 3e). To gauge the durability of the device, the S-TENG was placed under

mechanical compression and tapping for 6000 cycles (Fig. 3f). The device demonstrated excellent and consistent performance throughout the entire duration, speaking to its ability to perform over long periods.

The power density was also investigated by looking at the changes in voltage and current under different load resistances. From 0 MΩ to 1000 MΩ, the voltage increased to 11.6 V. With the increase in resistance, the decrease in current falls from 0.12 mA to 0.27 mA (Fig. 3g). The power distribution of this structure was measured, and the device demonstrated its ability to reach a peak power of 12.76 mW. Based on the dimensions set to a 4x4 $cm^2$ cloth, the device would be capable of generating a peak power per area of 7.98 W $m^{-2}$ at the matched load resistance of ~100 MΩ (Fig. S3).

The output performance of the S-TENG was systematically tested for its ability to sense the intensity of tapping, sensitivity to bending, and finally its ability to charge a capacitor. The S-TENG was subjected to finger tapping increasing the number of fingers from one finger to all five fingers (Fig. 3h). The measured voltage was lowest for one finger and increased with the highest voltage measured for five fingers. As demonstrated, within each cycle, there are distinct measurements across the different number of fingers ranging from 1.4 V (1 finger) to 5.1 V (5 fingers). Additionally, across each of these cycles in which the number of fingers was repeated, the voltages were consistently in the same general range for distinct electrical signals at each respective number of fingers (Fig. 3i). The output of the TENG was also carefully examined through a controlled bending and releasing at various predetermined angles. The fabricated device was attached to the index finger to measure the finger joint angle. From a fully extended state of 180º, electrical output was measured at 150º, 90º, and 60º. 90º index finger flexion is defined to be when the proximal interphalangeal joint undergoes flexion to a 90º angle. 150º flexion would be partway between 180º and 90º. 60º is when the index finger is fully bent. As demonstrated in Fig. 3j, there were distinct measurements for the voltage for each of the predefined deformations. At 150° flexion of the finger, the measured voltage was about

0.94 V. At 90° flexion, the measured voltage increased to 2.1 V. Finally, at multiple measurements of the finger flexion of 60°, the S-TENG outputted 3.4 V. These distinct and consistent measurements for specific finger extension and flexion demonstrate the potential to apply the S-TENG as a sensor for biomechanical movement under physical bending. As for proof-of-concept application, the S-TENG was explored as a human-machine interface to control a bionic robotic hand. As shown in Fig. 3k, the objective of this test was to demonstrate the ability of the S-TENG to control finger bending in the mechanical hand. In the test, the robotic finger was successfully bent under the stimulation of a linked S-TENG. To complement this setup, more S-TENG could be implemented and linked to more fingers forming a control panel to produce more complex tasks. More sensing information can be gained from the S-TENG to control fingers individually. Different sensing information can be processed and translated into various outputs such as which finger is bent and the degree to which it bends.

Finally, to examine the ability of the S-TENG as a power source harvesting biomechanical motion, the S-TENG was connected to a capacitor augmented by a rectifier. Driven by gentle tapping, the S-TENG is capable of charging 1μF, 2μF, and 10μF capacitors. **(**Fig. S4**)**. While maintaining the same tapping motion and speed without intensive effort from the user, the capacitors were charged in 14s, 19s, and 152s respectively. As a proof-of-concept application for this device, the S-TENG was integrated into a heartbeat sensor setup. The biomechanical work done by the tapping can be converted to electricity charging up the capacitors and in turn powering the sensor. More experimentation can be done to investigate the device's ability to simultaneously detect electrical signals due to the vibrations from the heartbeat and charge the capacitor to perform additional communication with other devices.

**2.4 Evaluation of fabric-drying performance**

Part of the allure of wearable sensors is derived from their practicality and minimal obstruction in the daily life of the user. To accomplish this in a wearable device involving textiles like the proposed S-TENG , air-permeability needs to be involved. One common reason is that with sweat glands producing sweat throughout the day, a method of wicking or evaporating the moisture at the site of the device would be very helpful for the user's comfort [16]. Taking a closer look by assessing the performance of the PCL electrospun cloth, in-depth moisture-wicking and evaporation tests were performed on the fabric in comparison with common commercially produced fabrics including Polyester, Cotton, and woven Polyethylene (PE). A droplet of water was placed on the fabric and its evaporation rate was measured across the 3 fabrics in addition to the PCL cloth with mesh sizes 30, 40, and 120 as well as 120 with plasma treatment (Methods and Fig. 4a). By inserting this water droplet, the processes of perspiration wicking and the evaporation of sweat are mimicked. Given that the objective of the wearable textile is to be worn on the skin with the fabric directly in contact with the skin surface, these tests can be an appropriate representation of the performance of the materials. As discussed in other papers, this woven fabric has a justified advantage as there is more efficient moisture-wicking in the direction of the yarn, spreading the droplet to the sides, and also elevating vertical moisture transport across the fabric [9]. Comparing all these fabrics in this paper, PCL at 120 mesh with plasma treatment outperformed all fabrics but woven PE (Fig. 4b-c). Thus, in the perspective of drying, the PCL textile has impressive qualities, superior to traditional materials such as Polyester and Cotton. Yet, it comes up short in comparison with woven PE. Temperature measurements were also taken beneath the woven PCL as well as cotton with four equidistant thermistors embedded to measure the lateral moisture and evaporative cooling performance of the textiles (Fig. 4d). The efficient moisture transport laterally promoting droplet spreading is observed given the uniform temperature across all 4 thermistors after a drastic initial drop (Fig. 4e). A similarly

sharp transition is also observed speaking to the fast evaporation of the material. This is contrasted by the cotton fibers which have exhibited uneven droplet spreading given the observably different temperatures between thermistors 6 and 8 which correspond to the same location as that of thermistors 2 and 4 in the PCL woven mesh. Additionally, the observed performance of the evaporation of the water droplet was much slower and gradual likely governed by the uneven droplet spread. Comparing these two fabrics, PCL's evaporative capability makes it a favorable fiber decreasing drying time, increasing comfort in its even temperature distribution, and also reducing energy consumption during instances such as tumble drying making it all the more economical [67].

**2.5 Outlook**

In comparison with other existing power-generating technologies, triboelectric nanogenerators, more specifically in this context, S-TENG is favorable. S-TENG makes use of affordable material with a relatively simple build and structure. Its lightweight and small size as well as its high output power relative to its weight and size make it easy to integrate into everyday clothing and wearable mediums.

Technically, the overall performance of the S-TENG can be augmented by enhancing the fabric used. As demonstrated in Fig. 4b and 4c, the 120 mesh PCL with plasma treatment has more favorable characteristics in the context of comfort in a sensor for a wearable device. While biodegradability and sustainability are important, the effectiveness of a sensor should also require more consideration of its durability and ability to endure and serve its purpose. The experiments demonstrated that the S-TENG had great durability in a lab setting when testing over many cycles with consistent results. However, more experimentation can be performed for other materials to optimize and balance between better durability and higher electrical power output. It is also worth noting that there may need to be more investigation and development in the circuitry to complement the development of

TENG in an industrial setting. Given that conventional electronics make use of high currents and lower voltages, there is an imbalance or mismatch with TENG as the S-TENG produces higher voltages and much lower currents. Existing solutions to transform and increase current while lowering voltage are typically bulkier. So, increasing the application of the S-TENG as a power source in a miniaturized system may require the development of a more suitable approach.

The triboelectric effect observed in the S-TENG enables energy harvesting and the production of electrical signals when the structure is subjected to deformation and compression. This method of power generation presents multi-faceted applications and can contribute to healthcare sensing needs. Scaled-down, a network of sensors can be employed to interpret complex motions and movements of a human through translation and processing of machine learning implementations. These small, light sensors can also be used to detect smaller, indiscernible, less obvious movements. This can be useful for patients with conditions such as muscular dystrophy who may lack the strength to press buttons or apply pressure on panels to communicate some of their needs with machines or other communication devices. The application with the human-machine interface involving the bionic hand is an example of an instance in which smaller, more subtle movements limited by the condition of the user can be translated to bigger, more complex movements to help them accomplish tasks they might not normally be able to perform. In addition to sensors, the ability to harvest energy in this S-TENG can also be utilized for areas such as electrical stimulating treatment for wound healing. With such a light and breathable patch that is also flexible and easily applied as a patch, the S-TENG can be used to complement a system designed to apply electrical stimulation to injuries.

## 2. Conclusion

In summary, we have successfully developed a soft textile TENG that is flexible, lightweight, and breathable while simultaneously capable of generating electricity which can be utilized as a power harvester and sensor. The device can effectively distinguish between different contact materials, is sensitive to varying force impact, and can produce electric output with great durability. The S-TENG is capable of harvesting mechanical energy in multiple forms including vibrations, impacts, bending, compressions, etc. The fabrication strategy that was implemented involving the electrospinning method is suitable for mass production and the materials itself is low-cost. Thus, the reported low-cost soft textile TENG introduces the comfortable appeal of being breathable and lightweight with its flexible integrity maintained through the liquid metal. We expect that this device could be an attractive starting point for more biomechanical sensors or energy sources to sensors integrated into the daily motions of an individual. In our demonstration of various electric performances with the fabricated device, further complementary development in terms of storing this energy can enable the S-TENG to power wearable electronic devices.

## 4. Experimental Section

### 4.1 Electrospinning process of PCL micro-fibers

Polycaprolactone was dissolved in a hexafluoro-2-propanol (HFIP) solution at 50°C through magnetic stirring, forming a viscous solution. The mass ratio of PCL to HFIP was kept at 1:10. Performed at room temperature, the solution was sent into a 20 mL syringe for electrospinning with an applied voltage at 18 kV, with the feeding rate of the solution set to 5 mL $h^{-1,}$ and the collecting distance of 15 cm. The electrostatically charged PCL microfibers were then collected on a stainless steel plate and subsequently removed for use.

### 4.2 Fabrication and Preparation of Eutectic gallium indium (Ni-EGaIn) layer

Gallium (99.99%) and In (99.99%) ingots were acquired from RotoMetals. A muffle furnace (ThermoFisher) was used to heat the EGaIn (74.5 wt% Ga and 25.5 wt% In) at 220ºC for 1 hour. A VWR mini vortexer was then used to thoroughly mix the liquid metal with 10 wt% Ni (99.5%, 5μm, US Research Nanomaterials) to the preferred rheological property for improved processability. Subsequently, to make a designed mask, the polyethylene terephthalate film was cut into a designed shape (outer length, 48.18 mm; inner length, 22.86 mm; line-width, 730 μm) with a laser cutting machine (ULTRA R5000, Universal Laser System). The Ni-EGaIn liquid metal was patterned into a thin substrate electrospun textile with the previously printed polyethylene terephthalate film mask.

### 4.3 Assembly of S-TENG

The layers of the EGaIn liquid metal were then patterned on the PCL textile. A second PCL textile was immediately placed on top to seal the liquid metal and allow it to oxidize and attach itself to both layers of fabric. A copper lead wire was attached on one side for electrical connection/output. For the plasma-treated S-TENG , the textile was put into a plasma reactor (PDC-001, Harrick) for surface modification. The chamber was thoroughly cleaned before operation. The power was set to be at maximum, and the treatment time was set to be 2 minutes.

### 4.4 Materials Characterization

The fluorescence images were collected by using a Zeiss Axio Observer Z1 inverted fluorescence microscope. The fluorescent marker was prepared by adding 0.1 wt% fluorescein sodium salt (Sigma Aldrich) to the PCL solution. Through the same process as regular PCL solution, fluorescent PCL electrospun fibers were also fabricated. The fluorescent marker was excited using a

488-nm laser channel with the PCL fibers given a green pseudo-color to emit. In terms of rheological characterization, all experiments were tested at a temperature of 25ºC. A rheometer (AR-2000, TA instruments) was used to measure the viscosity, storage modulus and loss modulus of the liquid metal. The sample was held by a steel plate (20 mm diameter) with a shear rate applied from 0 $s^{-1}$ to 100 $s^{-1}$. A sweep of stress ranging from 10 Pa to 10000 Pa was applied for the oscillation experiment.

### 4.5 Electrical Characterization of S-TENG

A control experiment was performed to verify the presence of the triboelectric effect converting the biomechanical motions into electric energy in the S-TENG. A Keithley system electrometer (6514) was used to measure voltage signals of the TENG. For the current signals, a Stanford low-noise current preamplifier (model SR570, Stanford) was employed. To test for stability of the S-TENG , the device was tested by a calibration electrodynamic transducer (Labworks, ET-126HF) at 20 Hz. For the standardized test, a flat plate with dimensions greater than that of the device was used. This plate is connected to an electrodynamic shaker system. The shaker system consists of a function generator (AFG1062, Newark), a linear power amplifier (PA-151, Labworks Inc.) as well as an electrodynamic transducer (ET_126HF, Labworks Inc.).

### 4.6 Rectifier/Capacitor Preparation

For measuring electrical output for power generation applications, a Schottky diode bridge rectifier (MBSK16SE) was used for a.c./d.c. conversion. Then, it was connected to electrolytic capacitors.

### 4.7 Bionic robotic-arm application

To demonstrate the capability of the S-TENG to work as a human-machine-interface

controlling a robotic arm, a mechanical hand (Hiwonder) was used. First, it was connected with the digital pins of a micro-controller (Adafruit QT Py - SAMD2). Second, the S-TENG was connected to a low-noise amplifier (AD620, Teyleten Robot), which was also connected with the the analog pins of a micro-controller. Finally, a on-board programe was made to control the bionic robotic-arm.

### 4.8 Preparation of artificial perspiration

To test the wicking abilities and performance of the cloth under moisture, artificial perspiration was used. A combination of 0.465 g NaCl (Sigma Aldrich), 3.87g 1M lactic acid solution (Alfa Aesar), 1.80 g Urea (Alfa Aesar), 1.37 g KCl (Sigma Aldrich), 0.756 g $NaHCO_3$ (Sigma Aldrich), 0.546 g 1 M $NH_3{\cdot}H_2O$ (Sigma Aldrich), 0.175 g $Na_2SO_4$ (Sigma Aldrich), and 0.0276 g uric acid (Alfa Aesar) were added in 3 L deionized water and mixed for 30 min.

### 4.9 Characterization of moisture drying properties of different fabrics

The characterization and testing of drying properties in fabrics were performed with a modified procedure based on the ISO 17617 standard (method B). Circular fabric test cloths dimensions were 85±2mm. The test cloths were kept at a maintained room temperature of 23.6 ± 0.3°C with a relative humidity of 40±5%. The ambient temperature and the relative humidity were measured for a day with a thermistor and hygrometer, respectively. Each sample was weighed in a Petri dish on a precision balance (Sartorius Secura 124-1S Analytical Balance). Using a micropipette, 0.25 ± 0.02 mL of distilled water was inserted at the center of the base of the Petri dish and covered by the test fabric cloth. The Petri dish along with the components placed in it was then exposed to the environment. Temperature and humidity were then measured during the length of exposure for this experiment. The change in weight due to the evaporation of water was measured over 2 minutes, and the drying time and drying rate (percentage $min^{-1}$) were calculated.

To measure how the spatial temperature distribution of the fabric is impacted by evaporation, these tests were performed once against using a Polystyrene plate with a temperature of 45° C. The dimensions of the plate had an area of 10 x 10 $cm^2$ and a thickness of 2cm. Four thermistors (TL1913SL) were placed onto the surface, and two were placed close and equidistant from the center (1cm). Another two were positioned radially outward spaced an additional 1 cm apart. At a sampling frequency of one sample per second, all thermistor data was logged with digital data longer, OM-CP-OCTPRO (Omega Instruments).

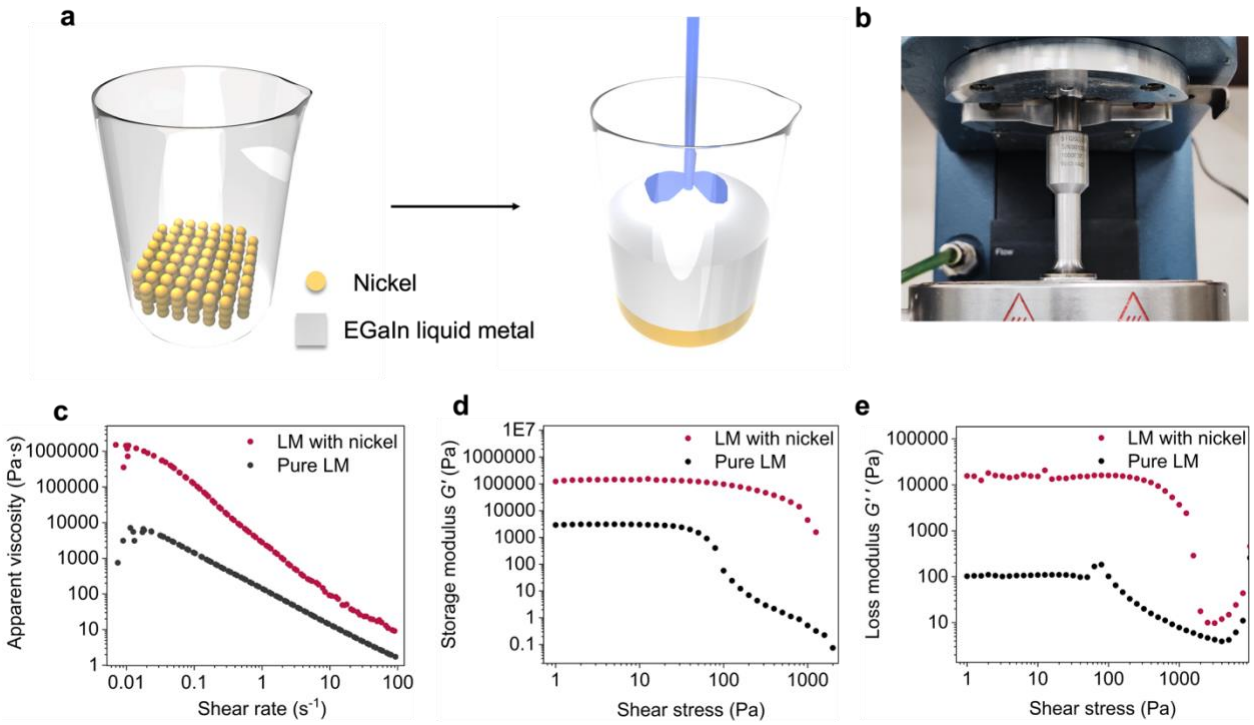


Fig. 1. Characterization of the Ni-EGaIn. (a) Mixing and preparation of the liquid metal electrode with the addition of Nickel particles. (b) Photograph of mechanical testing, measuring for the (c) Apparent viscosity, (d) Storage Modulus, and (e) Loss Modulus of the Ni-EGaIn liquid metal.

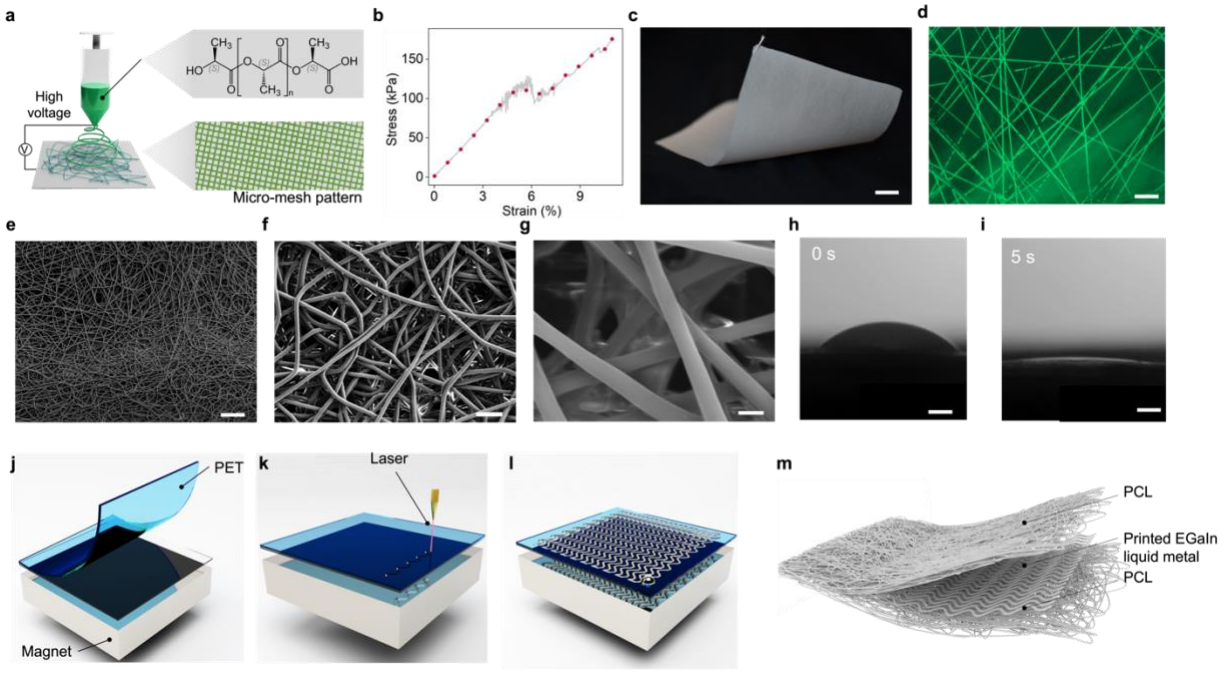


Fig. 2. Fabrication process of S-TENG . (a) Preparation of the PCL with a micro-mesh pattern. (b) Stress vs. Strain of PCL cloth with Young's modulus of 1.58 MPa. (c) Photograph showing the PCL cloth. (d) Fluorescent microscope image. SEM images of PCL cloth with scale bar: 100 μm (e), 20 μm (f), 2.5 μm(g). Liquid droplet contact angle image on plasma-treated PCL at 0 seconds (c) and 5 seconds (d). (j) Using the PET as a mold, laser cutting the shape (k) before inserting the liquid metal held down by the magnet (l). (m) Schematic of the assembled S-TENG .

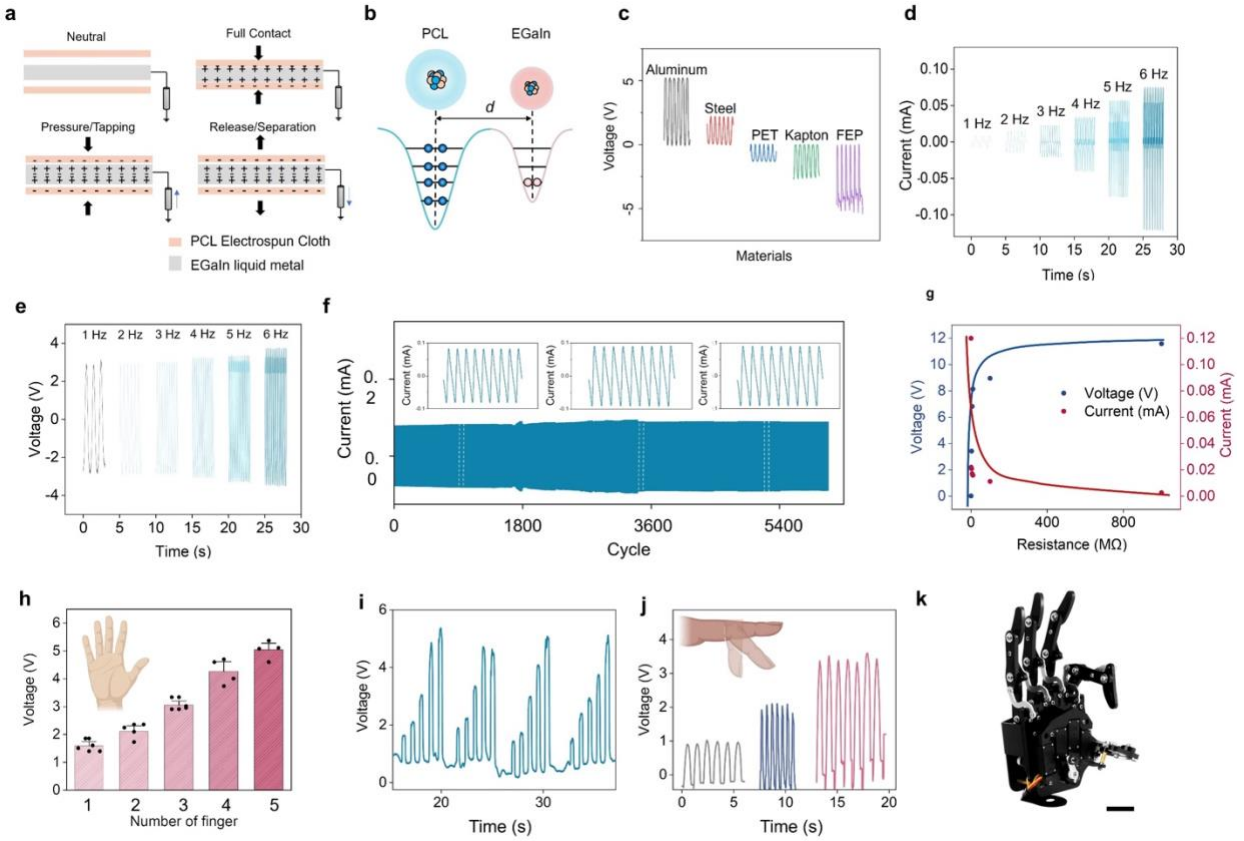


Fig. 3. Electrical and mechanical characterization of the S-TENG sensor. (a) Visualization of the S-TENG current and voltage process with (b) atomic-scale-electron-cloud potential-well model to describe contact electrification between PCL and EGaIn. (c) Voltage vs. contact material plot illustrating the distinct electrical output based on different materials. The current (d) and voltage (e) output under different tapping frequencies on the S-TENG surface. (f) The durability of the S-TENG output under continuous measurement over a period of 6000 cycles. The inset shows the enlarged view of the cycles at different time points marked by the double dashed line in the main plot. (g) Dependence of voltage and current on increasing resistance load conditions. (h) Voltage output of tapping under an increasing number of fingers. (i) Voltage output for cyclic finger tapping from one to five for four repetitions. (j) Voltage output due to varying degrees of finger bending angles. (k) Demonstration of the S-TENG as a human-machine-interface to control the bending of the bionic robotic hand.

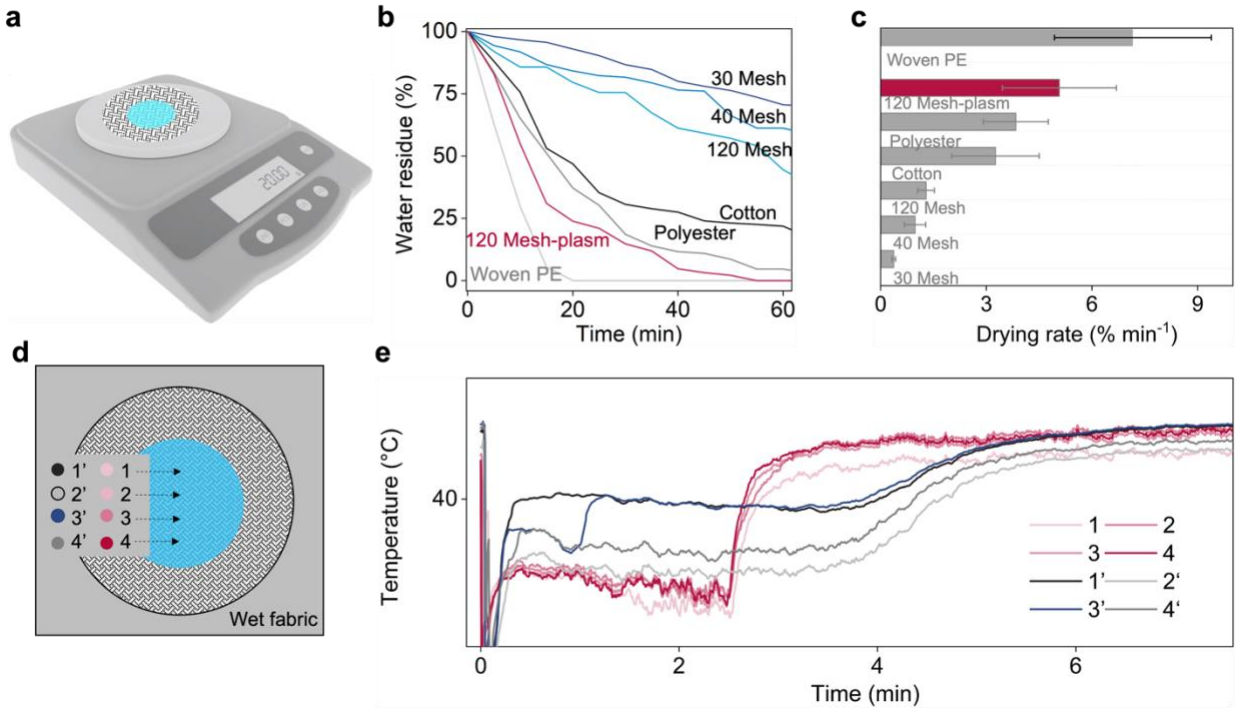


Fig. 4. Comparative drying and evaporative cooling performance of textiles. (a) Diagram of the experimental set-up used to measure the drying rate of water droplets placed into the fabric based on the weight change. Water residue (c) and drying rate (d) of woven PE fabric along with different commonly used textiles. Corresponding rates of commercial woven PE, Polyester, and Cotton used for comparison with the varying Mesh PCL textile. (d) Experimental diagram of the set-up employed to measure the spreading of lateral moisture and evaporative cooling performance of the textile. (e) Temperature measurements beneath PCL 120 mesh (1-4) and Cotton (1'- 4').

# 5. Appendices

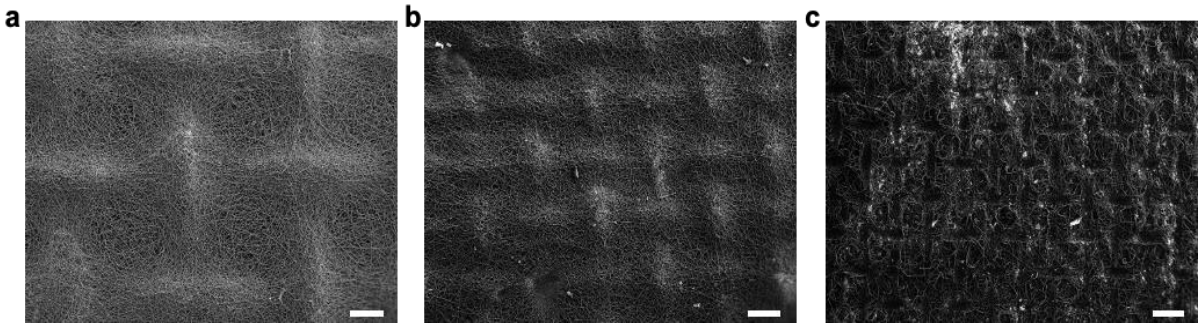


**Supplementary Figure 1. Morphology of PCL cloth at varying mesh sizes.** SEM image of PCL cloth with mesh size and scale bar: (a) 18, 240 μm (b) 35, 240 μm (c) 70, 200 μm.

The lateral dimensions of each opening in the 18-mesh cloth were 630μm by 710μm. For the 35-mesh cloth, the lateral dimensions were 300 μm by 250 μm. Finally, the 70-mesh cloth had lateral dimensions of 300 μm by 250 μm.

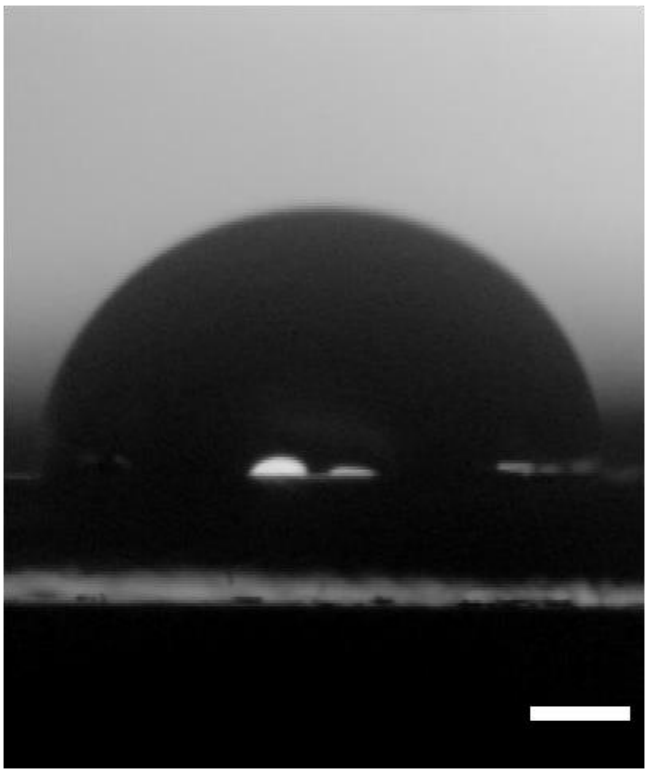

**Supplementary Figure 2. Droplet test on untreated PCL without plasma treatment.** This image is that of a water droplet placed onto the PCL cloth without undergoing plasma treatment. Due to the high surface energies, the droplet will adhere to the textile for a longer duration and have a much more delayed wicking and evaporating rate.

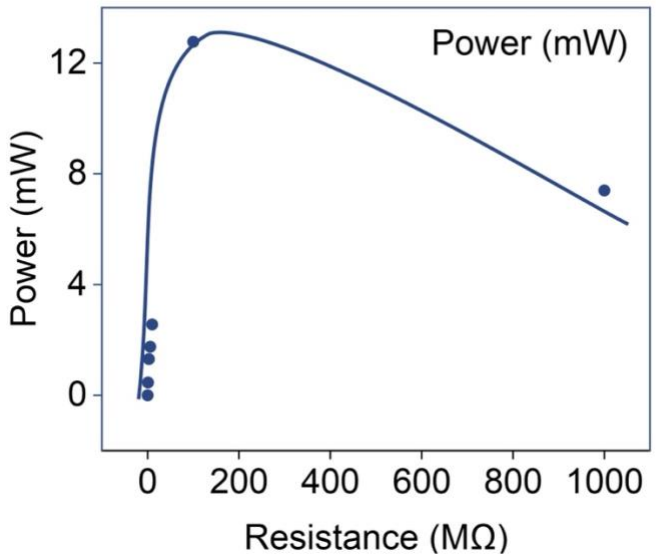


**Supplementary Figure 3. The power output under varying resistance**
Resistance was varied from 0 to 1 billion ohms and based on measurements of current and voltage of the S-TENG , this plot of the S-TENG power output over the increasing resistance was measured. The measured peak power was at 390 mW $m^{-2}$

**Supplementary Table 1. Price of PCL electrospun fiber and liquid metal electrode**

| Material Category | Price |
|---|---|
| PCL electrospun cloth fiber | $11 / g |
| Ni-eGaIn | $0.52 / g |

**Supplementary Table 2.** Water vapor transmission rate of different textile samples.

| TEXTILE CATEGORY | WATER VAPOR TRANSMISSION RATE |
|---|---|
| COTTON | 3.3% $min^{-1}$ |
| POLYESTER | 3.8% $min^{-1}$ |
| WOVEN PE | 7.2% $min^{-1}$ |
| 30 MESH PCL | 0.37% $min^{-1}$ |
| 40 MESH PCL | 0.98% $min^{-1}$ |
| 120 MESH PCL | 1.29% $min^{-1}$ |
| 120 MESH-PLASM PCL | 5.1% $min^{-1}$ |

The two textiles with the highest water vapor transmission rate was the woven Polethylene and the 120 mesh PCL cloth that underwent plasma treatment. This 120 Mesh-Plasm PCL was the cloth employed for the S-TENG .

## Bibliography

[1] A. Pantelopoulos, N. Bourbakis, A survey on wearable biosensor systems for health monitoring, IEEE Sensors Journal (2008) 4887-4890. https://doi.org/10.1109/iembs.2008.4650309.

[2] Z. Lou, L. Wang, G. Shen, Recent advances in smart wearable sensing systems, Adv. Mater. Technol. 3 (2018) 1800444. https://doi.org/10.1002/admt.201800444.

[3] Y. Khan, A.E. Ostfeld, C.M. Lochner, A. Pierre, A.C. Arias, Monitoring of vital signs with flexible and wearable medical devices, Adv. Mater. 28 (2016) 4373-4395. https://doi.org/10.1002/adma.201504366.

[4] Y. Yang, X. Yang, Y. Tan, Q. Yuan, Recent progress in flexible and wearable bio-electronics based on nanomaterials, Nano Res. 10 (2017) 1560-1583. https://doi.org/10.1007/s12274-017-1476-8.

[5] W. Zeng, L. Shu, Q. Li, S. Chen, F. Wang, X.-M. Tao, Fiber-based wearable electronics: a review of materials, fabrication, devices, and applications, Adv. Mater. 26 (2014) 5310-5336. https://doi.org/10.1002/adma.201400633.

[6] X. Peng, K. Dong, C. Ye, Y. Jiang, S. Zhai, R. Cheng, D. Liu, X. Gao, J. Wang, L. Wang Zhong, A breathable, biodegradable, antibacterial, and self-powered electronic skin based on all-nanofiber triboelectric nanogenerators, Sci. Adv. 6 (2020) eaba9624. https://doi.org/10.1126/sciadv.aba9624.

[7] K. Dong, X. Peng, J. An, A.C. Wang, J. Luo, B. Sun, J. Wang, Z.L. Wang, Shape adaptable and highly resilient 3D braided triboelectric nanogenerators as e-textiles for power and sensing, Nature Communications 11 (2020) 2868. https://doi.org/10.1038/s41467-020-16642-6.

[8] W. Fan, Q. He, K. Meng, X. Tan, Z. Zhou, G. Zhang, J. Yang, Z.L. Wang, Machine-knitted washable sensor array textile for precise epidermal physiological signal monitoring, Sci. Adv. 6 (2020) eaay2840. https://doi.org/10.1126/sciadv.aay2840.

[9] M. Alberghini, S. Hong, L.M. Lozano, V. Korolovych, Y. Huang, F. Signorato, S.H. Zandavi, C. Fucetola, I. Uluturk, M.Y. Tolstorukov, G. Chen, P. Asinari, R.M. Osgood, M. Fasano, S.V. Boriskina,

Sustainable polyethylene fabrics with engineered moisture transport for passive cooling, Nature Sustainability 4 (2021) 715-724. https://doi.org/10.1038/s41893-021-00688-5.

[10] G. Chen, Y. Li, M. Bick, J. Chen, Smart textiles for electricity generation, Chemical Reviews 120 (2020) 3668-3720. https://doi.org/10.1021/acs.chemrev.9b00821.

[11] Y. Zou, V. Raveendran, J. Chen, Wearable triboelectric nanogenerators for biomechanical energy harvesting. Nano Energy 77 (2020) 105303. https://doi.org/10.1016/j.nanoen.2020.105303.

[12] X. Ma, Z. Jiang, Y. Lin, Flexible energy storage devices for wearable bioelectronics. Journal of Semiconductors 42 (2021) 101602. https://doi.org/10.1088/1674-4926/42/10/101602.

[13] S.Z. Homayounfar, T.L. Andrew, Wearable sensors for monitoring human motion: a review on mechanisms, materials, and challenges, SLAS Technol. 25 (2020) 9-24. https://doi.org/10.1177/2472630319891128.

[14] Y. Zhou, X. Zhao, J. Xu, Y. Fang, G. Chen, Y. Song, S. Li, J. Chen, Giant magnetoelastic effect in soft systems for bioelectronics. Nature Materials, 20 (2021) 1670-1676. https://doi:10.1038/s41563-021-01093-1.

[15] G. Chen, X. Zhao, S. Andalib, J. Xu, Y. Zhou, T. Tat, K. Lin, J. Chen, Discovering giant magnetoelasticity in soft matter for electronic textiles. Matter, 4 (2021) 3725-3740. https://doi:https://doi.org/10.1016/j.matt.2021.09.012.

[16] X. Zhao, Y. Zhou, J. Xu, G. Chen, Y. Fang, T. Tat, X. Xiao, Y. Song, S. Li, J. Chen, Soft fibers with magnetoelasticity for wearable electronics. Nature Communications, 12 (2021) 6755. https://doi:10.1038/s41467-021-27066-1.

[17] G. Chen, Y. Zhou, Y. Fang, X. Zhao, S. Shen, T. Tat, A. Nashalian, J. Chen, Wearable Ultrahigh Current Power Source Based on Giant Magnetoelastic Effect in Soft Elastomer System. ACS Nano, 15 (2021) 20582-20589. https://doi:10.1021/acsnano.1c09274.

[18] X. Zhao, G. Chen, Y. Zhou, A. Nashalian, J. Xu, T. Tat, Y. Song, A. Libanori, S. Xu, S. Li, J. Chen, Giant Magnetoelastic Effect Enabled Stretchable Sensor for Self-Powered Biomonitoring. ACS Nano, 16 (2022) 6013-6022. https://doi:10.1021/acsnano.1c11350.

[19] J.J. Park, W.J. Hyun, S.C. Mun, Y.T. Park, O.O. Park, Highly Stretchable and Wearable Graphene Strain Sensors with Controllable Sensitivity for Human Motion Monitoring. ACS Applied Materials & Interfaces, 7 (2015) 6317-6324. https://doi:10.1021/acsami.5b00695.

[20] J. Ge, L. Sun, F.-R. Zhang, Y. Zhang, L.-A. Shi, H.-Y. Zhao, H.-W. Zhu, H.-L. Jiang, S.-H. Yu, A Stretchable Electronic Fabric Artificial Skin with Pressure-, Lateral Strain-, and Flexion-Sensitive Properties. Advanced Materials, 28 (2016) 722-728. https://doi:https://doi.org/10.1002/adma.201504239.

[21] A. Sadeqi, H.R. Nejad, F. Alaimo, H. Yun, M. Punjiya, S.R. Sonkusale, Washable Smart Threads for Strain Sensing Fabrics. IEEE Sensors Journal, 18 (2018) 9137-9144. https://doi:10.1109/JSEN.2018.2870640.

[22] K. Kim, M. Jung, S. Jeon, J. Bae, Robust and scalable three-dimensional spacer textile pressure sensor for human motion detection. Smart Materials and Structures, 28 (2019) 065019. https://doi:10.1088/1361-665x/ab1adf.

[23] A. Kiaghadi, S.Z. Homayounfar, J. Gummeson, T. Andrew, D. Ganesan, Phyjama: Physiological Sensing via Fiber-enhanced Pyjamas. Proc. ACM Interact. Mob. Wearable Ubiquitous Technol., 3 (2019) Article 89. https://doi:10.1145/3351247.

[24] S.K. Kundu, S. Kumagai, M. Sasaki, A Wearable Capacitive Sensor for Monitoring Human Respiratory Rate. Japanese Journal of Applied Physics, 52 (2013) 04CL05. https://doi:10.7567/jjap.52.04cl05.

[25] J. Cheng, O. Amft, P. Lukowicz, in: P. Floréen, A. Krüger, M. Spasojevic (Eds.) Pervasive Computing, Springer Berlin Heidelberg, Berlin, Heidelberg, 2010, pp. 319-336.

[26] Y.-N. Zheng, Z. Yu, G. Mao, Y. Li, D. Pravarthana, W. Asghar, Y. Liu, S. Qu, J. Shang, R.-W. Li, A Wearable Capacitive Sensor Based on Ring/Disk-Shaped Electrode and Porous Dielectric for Noncontact Healthcare Monitoring. Global Challenges, 4 (2020) 1900079. https://doi:https://doi.org/10.1002/gch2.201900079.

[27] Z. Zhang, J. Zhang, H. Zhang, H. Wang, Z. Hu, W. Xuan, S. Dong, J. Luo, A Portable Triboelectric Nanogenerator for Real-Time Respiration Monitoring. Nanoscale Research Letters, 14 (2019) 354. https://doi:10.1186/s11671-019-3187-4.

[28] L. Xie, X. Chen, Z. Wen, Y. Yang, J. Shi, C. Chen, M. Peng, Y. Liu, X. Sun, Spiral Steel Wire Based Fiber-Shaped Stretchable and Tailorable Triboelectric Nanogenerator for Wearable Power Source and Active Gesture Sensor. Nano-Micro Letters, 11 (2019) 39. https://doi:10.1007/s40820-019-0271-3.

[29] C. Yan, W. Deng, L. Jin, T. Yang, Z. Wang, X. Chu, H. Su, J. Chen, W. Yang, Epidermis-Inspired Ultrathin 3D Cellular Sensor Array for Self-Powered Biomedical Monitoring. ACS Applied Materials & Interfaces, 10 (2018) 41070-41075. https://doi:10.1021/acsami.8b14514.

[30] W.-S. Jung, M.-J. Lee, M.-G. Kang, H.G. Moon, S.-J. Yoon, S.-H. Baek, C.-Y. Kang, Powerful curved piezoelectric generator for wearable applications. Nano Energy, 13 (2015) 174-181. https://doi:https://doi.org/10.1016/j.nanoen.2015.01.051.

[31] J. Edmison, M. Jones, Z. Nakad, T. Martin, Proceedings. Sixth International Symposium on Wearable Computers2002, pp. 41-48.

[32] D. Larcher, J.M. Tarascon, Towards greener and more sustainable batteries for electrical energy storage. Nature Chemistry, 7 (2015) 19-29. https://doi:10.1038/nchem.2085.

[33] J. Chen, Y. Huang, N. Zhang, H. Zou, R. Liu, C. Tao, X. Fan, Z.L. Wang, Micro-cable structured textile for simultaneously harvesting solar and mechanical energy. Nature Energy, 1 (2016) 16138. https://doi:10.1038/nenergy.2016.138.

[34] X. Pu, L. Li, H. Song, C. Du, Z. Zhao, C. Jiang, G. Cao, W. Hu, Z.L. Wang, A Self-Charging Power Unit by Integration of a Textile Triboelectric Nanogenerator and a Flexible Lithium-Ion Battery for Wearable Electronics. Advanced Materials, 27 (2015) 2472-2478. https://doi:https://doi.org/10.1002/adma.201500311.

[35] F.-R. Fan, Z.-Q. Tian, Z. Lin Wang, Flexible triboelectric generator. Nano Energy, 1 (2012) 328-334. https://doi:10.1016/j.nanoen.2012.01.004.

[36] T. Bhatta, P. Maharjan, H. Cho, C. Park, S.H. Yoon, S. Sharma, M. Salauddin, M.T. Rahman, S.M.S. Rana, J.Y. Park, High-performance triboelectric nanogenerator based on MXene functionalized polyvinylidene fluoride composite nanofibers. Nano Energy, 81 (2021) 105670. https://doi:https://doi.org/10.1016/j.nanoen.2020.105670.

[37] W. Yang, W. Gong, C. Hou, Y. Su, Y. Guo, W. Zhang, Y. Li, Q. Zhang, H. Wang, All-fiber tribo-ferroelectric synergistic electronics with high thermal-moisture stability and comfortability. Nature Communications, 10 (2019) 5541. https://doi:10.1038/s41467-019-13569-5.

[38] Y.-C. Lai, Y.-C. Hsiao, H.-M. Wu, Z.L. Wang, Waterproof Fabric-Based Multifunctional Triboelectric Nanogenerator for Universally Harvesting Energy from Raindrops, Wind, and Human Motions and as Self-Powered Sensors. Advanced Science, 6 (2019) 1801883. https://doi:https://doi.org/10.1002/advs.201801883.

[39] Z. Wen, M.-H. Yeh, H. Guo, J. Wang, Y. Zi, W. Xu, J. Deng, L. Zhu, X. Wang, C. Hu, L. Zhu, X. Sun, L. Wang Zhong, Self-powered textile for wearable electronics by hybridizing fiber-shaped nanogenerators, solar cells, and supercapacitors. Science Advances, 2 (2016) e1600097. https://doi:10.1126/sciadv.1600097.

[40] S.K. Ghosh, D. Mandal, Synergistically enhanced piezoelectric output in highly aligned 1D polymer nanofibers integrated all-fiber nanogenerator for wearable nano-tactile sensor. Nano Energy, 53 (2018) 245-257. https://doi:https://doi.org/10.1016/j.nanoen.2018.08.036.

[41] S. Anwar, M. Hassanpour Amiri, S. Jiang, M.M. Abolhasani, P.R.F. Rocha, K. Asadi, Piezoelectric Nylon-11 Fibers for Electronic Textiles, Energy Harvesting and Sensing. Advanced Functional Materials, 31 (2021) 2004326. https://doi:https://doi.org/10.1002/adfm.202004326.

[42] X. Guan, B. Xu, J. Gong, Hierarchically architected polydopamine modified BaTiO3@P(VDF-TrFE) nanocomposite fiber mats for flexible piezoelectric nanogenerators and self-powered sensors. Nano Energy, 70 (2020) 104516. https://doi:https://doi.org/10.1016/j.nanoen.2020.104516.

[43] A. Lund, K. Rundqvist, E. Nilsson, L. Yu, B. Hagström, C. Müller, Energy harvesting textiles for a rainy day: woven piezoelectrics based on melt-spun PVDF microfibres with a conducting core. npj Flexible Electronics, 2 (2018) 9. https://doi:10.1038/s41528-018-0022-4.

[44] Y. Qin, X. Wang, Z.L. Wang, Microfibre–nanowire hybrid structure for energy scavenging. Nature, 451 (2008) 809-813. https://doi:10.1038/nature06601.

[45] G. Khandelwal, N.P. Maria Joseph Raj, S.-J. Kim, Triboelectric nanogenerator for healthcare and biomedical applications. Nano Today, 33 (2020) 100882. https://doi:https://doi.org/10.1016/j.nantod.2020.100882.

[46] J. Chen, Z.L. Wang, Reviving Vibration Energy Harvesting and Self-Powered Sensing by a Triboelectric Nanogenerator. Joule, 1 (2017) 480-521. https://doi:https://doi.org/10.1016/j.joule.2017.09.004.

[47] Y. Su, T. Yang, X. Zhao, Z. Cai, G. Chen, M. Yao, K. Chen, M. Bick, J. Wang, S. Li, G. Xie, H. Tai, X. Du, Y. Jiang, J. Chen, A wireless energy transmission enabled wearable active acetone biosensor for non-invasive prediabetes diagnosis. Nano Energy, 74 (2020) 104941. https://doi:https://doi.org/10.1016/j.nanoen.2020.104941.

[48] Y. Su, J. Wang, B. Wang, T. Yang, B. Yang, G. Xie, Y. Zhou, S. Zhang, H. Tai, Z. Cai, G. Chen, Y. Jiang, L.-Q. Chen, J. Chen, Alveolus-Inspired Active Membrane Sensors for Self-Powered

Wearable Chemical Sensing and Breath Analysis. ACS Nano, 14 (2020) 6067-6075. https://doi:10.1021/acsnano.0c01804.

[49] Z. Zhou, L. Weng, T. Tat, A. Libanori, Z. Lin, L. Ge, J. Yang, J. Chen, Smart Insole for Robust Wearable Biomechanical Energy Harvesting in Harsh Environments. ACS Nano, 14 (2020) 14126-14133. https://doi:10.1021/acsnano.0c06949.

[50] R. Zhang, H. Olin, Material choices for triboelectric nanogenerators: A critical review. EcoMat, 2 (2020) e12062. https://doi:https://doi.org/10.1002/eom2.12062.

[51] K. Deshmukh, M. Basheer Ahamed, R.R. Deshmukh, S.K. Khadheer Pasha, P.R. Bhagat, K. Chidambaram, 3 - Biopolymer Composites With High Dielectric Performance: Interface Engineering, in: K.K. Sadasivuni, D. Ponnamma, J. Kim, J.J. Cabibihan, M.A. AlMaadeed (Eds.) Biopolymer Composites in Electronics, Elsevier2017, pp. 27-128.

[52] J. Yin, Q. Zhao, Y. Shen, B. He, P(LLA-co-PDO) copolymers with random and block architectures: Synthesis and characterizations. Journal of Applied Polymer Science, n/a (2022) 52410. https://doi:https://doi.org/10.1002/app.52410.

[53] O.C. Ernst, K. Böttcher, D. Fischer, D. Uebel, T. Teubner, T. Boeck, Morphogenesis of Liquid Indium Microdroplets on Solid Molybdenum Surfaces during Solidification at Normal Pressure and under Vacuum Conditions. Langmuir, 38 (2022) 762-768. https://doi:10.1021/acs.langmuir.1c02744.

[54] A.R. Jacob, D.P. Parekh, M.D. Dickey, L.C. Hsiao, Interfacial Rheology of Gallium-Based Liquid Metals. Langmuir, 35 (2019) 11774-11783. https://doi:10.1021/acs.langmuir.9b01821.

[55] L. Majidi, D. Gritsenko, J. Xu, Gallium-Based Room-Temperature Liquid Metals: Actuation and Manipulation of Droplets and Flows. Frontiers in Mechanical Engineering, 3 (2017).

[56] J. Xue, T. Wu, Y. Dai, Y. Xia, Electrospinning and Electrospun Nanofibers: Methods, Materials, and Applications. Chemical Reviews, 119 (2019) 5298-5415. https://doi:10.1021/acs.chemrev.8b00593.

[57] H.-W. Chen, M.-F. Lin, Characterization, Biocompatibility, and Optimization of Electrospun SF/PCL/CS Composite Nanofibers. Polymers, 12 (2020). https://doi:10.3390/polym12071439.

[58] K. Saeed, S.-Y. Park, H.-J. Lee, J.-B. Baek, W.-S. Huh, Preparation of electrospun nanofibers of carbon nanotube/polycaprolactone nanocomposite. Polymer, 47 (2006) 8019-8025. https://doi:https://doi.org/10.1016/j.polymer.2006.09.012.

[59] K. Miller, J.E. Hsu, L.J. Soslowsky, 6.618 - Materials in Tendon and Ligament Repair, in: P. Ducheyne (Ed.) Comprehensive Biomaterials, Elsevier, Oxford, 2011, pp. 257-279.

[60] M. Bartnikowski, T.R. Dargaville, S. Ivanovski, D.W. Hutmacher, Degradation mechanisms of polycaprolactone in the context of chemistry, geometry and environment. Progress in Polymer Science, 96 (2019) 1-20. https://doi:https://doi.org/10.1016/j.progpolymsci.2019.05.004.

[61] H. Tsuji, T. Ishizaka, Blends of aliphatic polyesters. VI. Lipase-catalyzed hydrolysis and visualized phase structure of biodegradable blends from poly(ε-caprolactone) and poly(l-lactide). International Journal of Biological Macromolecules, 29 (2001) 83-89. https://doi:https://doi.org/10.1016/S0141-8130(01)00158-1.

[62] M.A. Woodruff, D.W. Hutmacher, The return of a forgotten polymer—Polycaprolactone in the 21st century. Progress in Polymer Science, 35 (2010) 1217-1256. https://doi:https://doi.org/10.1016/j.progpolymsci.2010.04.002.

[63] S. Houshyar, G.S. Kumar, A. Rifai, N. Tran, R. Nayak, R.A. Shanks, R. Padhye, K. Fox, A. Bhattacharyya, Nanodiamond/poly-ε-caprolactone nanofibrous scaffold for wound management. Materials Science and Engineering: C, 100 (2019) 378-387. https://doi:https://doi.org/10.1016/j.msec.2019.02.110.

[64] R. Guo, X. Wang, H. Chang, W. Yu, S. Liang, W. Rao, J. Liu, Ni-GaIn Amalgams Enabled Rapid and Customizable Fabrication of Wearable and Wireless Healthcare Electronics. Advanced Engineering Materials, 20 (2018) 1800054. https://doi:https://doi.org/10.1002/adem.201800054.

[65] X. Wang, R. Guo, B. Yuan, Y. Yao, F. Wang, J. Liu, 2018 40th Annual International Conference of the IEEE Engineering in Medicine and Biology Society (EMBC)2018, pp. 3276-3279.

[66] Y. Zhou, W. Deng, J. Xu, J. Chen, Engineering materials at the nanoscale for triboelectric nanogenerators Cell Reports Physical Science, 1 (2020). https://doi:10.1016/j.xcrp.2020.100142.

[67] J. Allwood, S. Laursen, C. Rodríguez, N. Bocken, Well Dressed? The Present and Future Sustainability of Clothing and Textiles in the United Kingdom, University of Cambridge2006.